Heterogeneous distribution of exocytotic microdomains in adrenal chromaffin cells resolved by high-density diamond ultra-microelectrode arrays

S. Gosso,M. Turturici,C. Franchino,E. Colombo,A. Pasquarelli,E. Carbone,V. Carabelli

Heterogeneous distribution of exocytotic microdomains in adrenal chromaffin cells resolved by high-density diamond ultra-microelectrode arrays

THE JOURNAL OF PHYSIOLOGY (2014) 592
DOI: 10.1113/jphysiol.2014.274951

Heterogeneous distribution of exocytotic microdomains in adrenal chromaffin cells resolved by high-density diamond ultramicroelectrode arrays

Sara Gosso, Marco Turturici*, Claudio Franchino, Elisabetta Colombo[§◊], Alberto Pasquarelli[§],

Emilio Carbone, Valentina Carabelli†

Department of Drug Science and Technology, NIS Center, University of Torino, 10125 Torino, Italy

* Department of Neuroscience University of Torino, 10125 Torino, Italy

§ Institute of Electron Devices and Circuit, University of Ulm, 89069 Ulm, Germany

◊ Present address: Neuroscience and Brain Technologies, Italian Institute of Technology, 16163 Genova, Italy

† *Corresponding author:* Valentina Carabelli
Department of Drug Science and Technology
Lab of Cellular Physiology & Molecular Neuroscience
Corso Raffaello 30
10125 - Torino, Italy
tel.: +39.011.670.8488
fax: +39.011.670.8498
e-mail: valentina.carabelli@unito.it

Running title: Diamond arrays for resolving spatial mapping of exocytosis

Keywords: exocytosis, chromaffin, micro-electrode arrays

Key points (149 words)

- A planar nanocrystalline diamond array with nine ultra-microelectrodes (9-Ch NCD-UMEA) has been designed for high-spatial resolution of amperometric recordings in single chromaffin cells.
- The 9-Ch NCD-UMEA operates in voltammetric and amperometric mode to reveal low doses of adrenaline, dopamine and serotonin. The lowest detectable concentration of adrenaline is ~5 μM.
- Using mouse and bovine chromaffin cells, single quantal exocytotic events are recorded from nine microareas of 12-27 μm^2. We found an excellent correspondence with recordings from the cell apex with carbon-fiber electrodes.
- In the bovine, secretion is heterogeneous. There are areas of high- and medium-activity covering 54% of the cell surface and areas of low- and no-activity covering the remaining. The "non-active zones" (silent) cover 24% of the cell surface and persist for minutes as the "active zones".
- The 9-Ch NCD-UMEA brings new insights in the spatial mapping of secretory sites in chromaffin cells.

Abstract

Here we describe the ability of a high-density diamond microelectrode array targeted to resolve multi-site detection of fast exocytotic events from single cells. The array consists of nine boron-doped nanocrystalline diamond ultra-microelectrodes (9-Ch NCD-UMEA) radially distributed within a circular area of the dimensions of a single cell. The device can be operated in voltammetric or chronoamperometric configuration. Sensitivity to catecholamines, tested by dose-response calibrations, set the lowest detectable concentration of adrenaline to ~5 μM. Catecholamine release from bovine or mouse chromaffin cells could be triggered by electrical stimulation or external KCl-enriched solutions. Spikes detected from the cell apex, using carbon fiber microelectrodes, showed an excellent correspondence with events measured from the cell bottom by the 9-Ch NCD-UMEA, confirming the ability of the array to resolve single quantal secretory events. Subcellular localization of exocytosis was provided by assigning each quantal event to one of the nine channels based on its location. The resulting mapping highlights the heterogeneous distribution of secretory activity in cell micro-domains of 12-27 μm^2. In bovine chromaffin cells, secretion was highly heterogeneous with zones of high-medium activity in 54% of cell surface and zones of low- or no-activity in the remaining. The "non-active" ("silent") zones covered 24% of the total and persisted for 6-8 min, indicating stable location. The 9-Ch NCD-UMEA appears thus suitable for investigating the microdomain organization of neurosecretion with high-spatial resolution.

Abbreviations NCD, nanocrystalline diamond; UMEA, ultra-microelectrode array; CFE, carbon fiber electrode; ITO, indium-tin-oxide; BEN, bias-enhanced nucleation; HFCVD, hot filament chemical vapor deposition; RIE, reactive ion etching; MCC, mouse chromaffin cell; BCC, bovine chromaffin cell.

Introduction

Exocytosis is an essential step for neurotransmission, allowing the vesicle content to be released into the extracellular space. Focusing on oxidizable neurotransmitters, the quantal nature of exocytosis can be uncovered by amperometric recordings. Properly polarized electrodes are placed next to the secreting cell and the electrochemically active surface of the electrode gives rise to a transient oxidation current (spike), which reflects the time course of vesicle fusion and release of oxidizable neurotransmitter molecules (Wightman *et al.*, 1991; Chen *et al.*, 1994; Wightman *et al.*, 1995; Xin & Wightman, 1998). Main features of this technique are: i) the sub-millisecond temporal resolution, ii) the high signal-to-noise ratio, which allows to estimate the quantity of released molecules and the fusion pore formation, and iii) the ability to provide a direct measure of exocytosis, independent of vesicle retrieval (endocytosis) (Haller *et al.*, 1998).

Amperometric spikes using carbon fiber electrodes (CFEs) are routinely detected on catecholamine-secreting chromaffin cells containing large-dense core vesicles (Wightman *et al.*, 1991), but they can also be associated to the fusion of small synaptic vesicles in midbrain dopaminergic neurons (Staal *et al.*, 2004). CFEs are easily shaped by a scalpel blade but have two main disadvantages: *1)* their usage is limited to single-cell experiments and *2)* the large electrode active surface (~ 45 μm^2) severely hinders the recording from different micro-areas of the same cell. This latter issue, can be partially overcome by using small-sized CFEs (~2 μm diameter) carefully placed in different areas of the cell to reveal discontinuity of secretory events (Schroeder *et al.*, 1994). This approach, however, is time consuming and does not furnish a quantitative view of the regional diversities of chromaffin cell secretion.

To overcome these drawbacks several attempts have been made to realize either planar multielectrode arrays for simultaneous recordings from different cells (Ayers *et al.*, 2010; Barizuddin *et al.*, 2010; Carabelli *et al.*, 2010; Kim *et al.*, 2012) or multi-site arrays for electrochemical detection from a single cell, to improve the spatial resolution of secretory events (Dias *et al.*, 2002; Hafez *et al.*, 2005; Zhang *et al.*, 2008; Kisler *et al.*, 2012; Lin *et al.*, 2012). To fulfill the second task, two CFE prototypes have been recently assembled, one made of seven tightly packed carbon fibers (Zhang *et al.*, 2008) and one with 8-15 carbon micro-rings assembled on a single tip (Lin *et al.*, 2012). Despite the increased spatial resolutions these microelectrodes possesses the same advantages and drawbacks of classical CFEs. Concerning the planar multielectrode arrays with high-spatial resolution, only 4-channels planar arrays have been so far realized based on different conducting materials. Platinum (Dias *et al.*, 2002; Hafez *et al.*, 2005), and more recently nitrogen-doped diamond-like carbon, thin gold films and indium-tin-oxide (ITO) have been employed (Kisler *et al.*, 2012). All these arrays

could detect fast amperometric spikes with high-time resolution except ITO that exhibited a significantly reduced sensitivity to catecholamines.

Given the importance of resolving the molecular events controlling the exocytotic machinery at higher-spatial resolution, we recently fabricated a high-density diamond ultra-microelectrode array with nine recording channels (9-Ch NCD-UMEA), whose overall area fits the size of a bovine chromaffin cell (Colombo *et al.*, 2011). The microchip relies on the outstanding properties of boron-doped nanocrystalline diamond (Carabelli *et al.*, 2010; Gao *et al.*, 2011), i.e., biocompatibility, chemical inertness and stability, electrochemical sensitivity, optical transparency and wide potential window for water dissociation, thus allowing the electrochemical detection in both anodic and cathodic range (Pasquarelli *et al.*, 2011).

Here we show that, when tested on bovine and mouse chromaffin cells, the 9-Ch NCD-UMEA possesses the same temporal resolution and catecholamine sensitivity of CFEs and is thus able to fully resolve amperometric spikes >8 pA arising from areas as small as 12 μm^2. We found that the overall frequency of catecholamine release measured by all electrodes was significantly higher than CFEs, and proportional to the electrochemically active surface of the microelectrodes. Under these conditions, we show that the nine electrodes can independently reveal zones of variable secretory activity, ascribed uniquely to different frequency of release, while temporal and quantitative spike parameters are unmodified among the secreting zones. The 9-Ch NCD-UMEA uncovers zones of high- and medium-activity distributed over 52% of the total area while zones of low- or no-activity cover the remaining part and persisted for minutes. The "silent zones" covered 24% of the total area and furnished a quantitative estimate of early observations by Schroeder et al., 1994 on the existence of stable "inactive release zones" of secretion in BCCs. The 9-Ch NCD-UMEA, thus provides a user-friendly tool for resolving amperometric signals with high-spatial resolution that can be employed to investigate the heterogeneous distribution of secretory sites on chromaffin membrane surface (Schroeder *et al.*, 1994; Robinson *et al.*, 1995; Klingauf & Neher, 1997; Carabelli *et al.*, 1998).

Methods

Ethical approval

All experimental protocols were approved by the University of Torino Animal Care and Use Committee, Torino, Italy and were performed according to the National Guide for the Care and Use of Laboratory Animals adopted by the Italian Ministry of Health. Every effort was made to minimize animal suffering and the number of animals used. For removal of tissues, mice were deeply anaesthetized with CO_2 inhalation and rapidly killed by cervical dislocation. Bovine adrenal glands were instead provided by the municipal slaughterhouse of Torino. They were isolated during the

removal of the internal organs of the dead animal under veterinary supervision and with permission of the competent authorities.

Device fabrication and design

The 9-Ch NCD-UMEA is realized by growing the NCD thin-film on a double side polished sapphire wafer (Epistone, 2″ DSP wafers), after an initial bias-enhanced nucleation process, which ensures strong covalent adhesion of the NCD film on the substrate (Colombo *et al.*, 2011). A 200 nm NCD intrinsic layer is grown by means of hot filament chemical vapour deposition (HFCVD). Then, e-beam lithography and reactive ion etching (RIE) in argon/oxygen plasma were used to define the nine microelectrodes geometry. The etching process was performed down to the sapphire substrate, to achieve the electrical insulation between the ultra-microelectrodes (>200 GΩ). Onto the intrinsic NCD tracks a ~250 nm boron-doped NCD layer was deposited by microwave plasma CVD, then the surface was treated with chromosulphuric acid in order to remove possible graphitic content and to obtain an oxygen surface termination. Notice that the BEN process involves the deposition of a thin silicon interlayer, which reduces the optical transparency of the 9-Ch NCD-UMEA, thus limiting its employment for fluorescence measurements.

Ohmic contacts were realized by Ti/Au deposition and optical lithography; a Si_3N_4 passivation layer (1 μm) was deposited by plasma enhanced CVD, because of its mechanical and chemical resistance. In the passivation layer, we opened a central hole (22 μm in diameter), in correspondence of the 9 microelectrodes, by optical lithography and RIE. The chip was assembled underneath a carrier board by flip-chip bonding with conductive epoxy and finally a glass ring was glued on the device to provide a perfusion chamber (150 μl) for the cells. Fig. 1 shows the chip assembled onto the carrier board (A), an enlarged view of the perfusion chamber (B) and the details of the 9 ultra-microelectrodes array in the round central hole (C) with a mouse chromaffin cell positioned on top of the electrodes by means of a glass patch-clamp pipette as indicated.

Isolation and culture of mouse chromaffin cells

Chromaffin cells of the adrenal medulla were obtained from young (1–3 months) C57BL/6N mice killed by cervical dislocation, and cultured as previously described (Marcantoni *et al.*, 2009). Medulla digestion was achieved for 28 min at 37 °C in a Dulbecco's modified Eagle's medium (DMEM) containing (in mM): 1.5 l-cysteine, 1 $CaCl_2$, 0.5 EDTA and 20 U/ml of papain (Worthington Biochemical Corp., Lakewood, NJ) and washing two times with a Locke's solution containing 1 mM $CaCl_2$ and 10 mg/ml bovine serum albumin (BSA). Cells were then resuspended in 2 ml DMEM supplemented with 15% fetal calf serum (FCS) and plated in four-well plastic dishes previously treated with 5% BSA. in order to avoid adhesion. After 1 h, 1.8 ml of DMEM supplemented with 15% fetal calf serum (FCS) (Invitrogen, Grand Island, NY), 50 IU/ml penicillin,

and 50 μg/ml streptomycin (Invitrogen) was added. Cells were then incubated at 37° C in a water-saturated atmosphere with 5% CO_2 and used within 2–4 days after plating.

Isolation and culture of bovine chromaffin cells

Bovine chromaffin cells were isolated as previously described (Carabelli *et al.*, 1998). Adrenal glands from 6 to 18-month-old cows just sacrificed were rapidly transported to the culture unit in Locke buffer containing (mM): 154 NaCl, 5.6 KCl, 3.5 $NaHCO_3$, 5.6 glucose, and 10 HEPES (pH 7.3 with NaOH). After controlling the integrity of the gland, the medulla digestion started by injecting 3 ml of Locke solution containing 0.2% collagenase (Sigma Chemical, St. Louis, MO), 1.7% hyaluronidase (Sigma), 0.5% bovine serum albumin (Sigma) and 0,15% Dnase I (Sigma). This was repeated three times at 30 min intervals while glands were kept at 37°C. Separation of the medulla from the cortex was performed manually with a disposable blade. Digestion solution was washed, and the tissue suspension was filtered with a nylon mesh (217 μm pore) and centrifuged at 900 rpm for 12 min at room temperature.

The surnatant and the upper pellet of erythrocytes was removed, while the pellet of chromaffin resuspended in DMEM (GIBCO, Grand Island, NY) and filtered with a nylon mesh (80 μm pore).

Cells were plated at a density of 1.5 10^4/ml in BSA-treated plastic dishes, to avoid cell adhesion, and incubated at 37 °C in a water-saturated 5% CO_2 atmosphere. The culture medium contained: DMEM, fetal calf serum (15%) (GIBCO), penicillin 50 IU/ml, streptomycin 50 μg/ml (GIBCO). Cells were used within 2–4 days after plating.

Amperometric recordings with 9-Ch NCD-UMEA and CFEs

In order to detect amperometric spikes due to the oxidation of secreted catecholamines, mouse (or bovine) chromaffin cells were removed from non-adherent BSA-treated dishes and centrifuged for 4 min at 900 rpm. Then the pellet was suspended in a physiological solution containing (mM): 128 NaCl, 2 $MgCl_2$, 10 HEPES, 10 glucose, 10 $CaCl_2$, 4 KCl. Finally 50 μl of the cell suspension was placed in the perfusion chamber of the device. After waiting few seconds for the cells to deposit on the bottom, we used a piezo-electric driven micromanipulator to position one cell on the central hole, where the nine ultra-microelectrodes emerge. We used two different strategies to elicit catecholamine release: either an electrical stimulation of ±2 V square pulses of 50 ms duration, provided through the nine planar recording electrodes, or a KCl-enriched solution containing (mM): 100 NaCl, 2 $MgCl_2$, 10 HEPES, 10 glucose, 30 KCl, 10 $CaCl_2$. Settings of the electrical stimulation protocol were adjusted to obtain secretory responses comparable to those evoked by extracellular KCl-enriched solution. To oxidize released catecholamines, both NCD-MEA electrodes and CFEs were polarized at +800 mV in amperometric mode and signals were monitored along with 2 min recordings. All

potentials are measured vs. the Ag/AgCl reference electrode. Amperometric recordings were analyzed by means of Igor macros, as previously described (Carabelli *et al.*, 2007).

National Instruments hardware and software were employed for data acquisition and extracellular stimulation. Signal acquisition was performed at 16 bit resolution with a sampling rate of 4 kHz per channel and filtered at 1 kHz with a 6^{th} order Bessel low-pass filter.

The electrical noise of each microelectrode was determined in spikes-free trace segments of 10 s duration. The noise level was evaluated and then averaged over the nine electrodes, leading to a mean background noise amplitude of 6 ± 1 pA peak-to-peak, in good agreement with previous devices (Berberian *et al.*, 2009). Following this, in the software routine the amperometric spikes were considered fully-resolved if their amplitude was >8 pA. It is worth noticing that the noise level of the recording system is set by the dynamic range of the acquisition parameters (16 bit resolution and ± 10 V input range) and not by the NCD electrodes or the front-end electronics. In fact by reducing the dynamic range, the noise level scales down linearly by more than one decade. The reason for using a large dynamic range was to shorten the time the amplifiers recover their linear operation after they saturate during strong electrical stimulation. Since the system cannot detect signals until recovery the linear operation, we have chosen to shorten the recovery time in order to maximize the collection of secretory events immediately after each stimulus using a large dynamic range, despite it increases the background noise. The same conditions were adopted also when using the chemical stimulation.

Except otherwise indicated, data are given as mean ± S.E.M.

Subcellular spatial mapping of exocytosis

To map the spatial distribution of exocytotic events on the chromaffin cells surface, we developed a MatLab routine which assigned each detected amperometric spike to one of the nine microelectrodes. To provide a graphical representation of the exocytotic events in distinct subcellular microdomains, the number of spikes revealed by each microelectrode was converted in a color scale and the resulting color assigned to the area of a 44x44 square grid occupied by the microelectrode (see Fig. 7). The routine analyzed also the raster plot of the 9-Ch recordings to identify spikes simultaneously detected by neighboring electrodes. To the purpose, we assumed that two or more spikes were simultaneous, and thus corresponding to the same exocytotic event, if their temporal shift was comparable with the time spent by catecholamines to diffuse from the release site to the ultra-microelectrodes. Given that the cell was positioned on top of the electrodes and the distance between the cell (release site) and the ultra-microelectrodes is negligible compared to the average distance between ultra-microelectrodes (Δl ~6 μm), the time required for the catecholamines to reach the

electrodes is $\Delta t = \frac{\Delta l^2}{6D}$ (Schroeder *et al.*, 1994), where $D = 6 \cdot 10^{-6} \frac{cm^2}{s}$ (Gerhardt & Adams, 1982) is the diffusion coefficient of catecholamines in aqueous solution. Thus, when the difference in time between the spike maxima was less than 10 ms, the recordings were identified as corresponding to a single exocytotic event and the routine assigned the spike to the microelectrode that detected it with larger amplitude.

At variance with Hafez et al (2005), who localized simultaneous events on the basis of random walk simulation and fitting the position of release events detected by more than two electrodes, we have chosen not to interpolate events detected from more than one electrode. This is because the spatial resolution of the device was about 27 μm^2, corresponding to the area of the largest electrodes (Ch 3, 6 and 9 in Fig. 1C), but the electrodes were separated by more or less a similar average area (~25 μm^2), so the error was comparable to the resolution of the instrument. Finally, since three of the nine electrodes had a larger area (Fig. 1C), the number of events detected by each electrode was normalized to the surface area.

Cleaning procedure of the array

Robustness and stability of the proposed device make the 9-Ch NCD-UMEA an extreme versatile tool for in vitro recordings from living cells. To this purpose, the prototype could be easily cleaned and re-used many times without damage. The cleaning procedure started by washing the device with an enzymatic detergent (Tergazyme, Sigma), to remove organic residues due to the presence of cells in the perfusion chamber. The device was immersed in a solution containing 1% Tergazyme in distilled water for 4 h. The solution was heated (35° C) and stirred to facilitate the removal of the organic material deposited on the nine microelectrodes. After 4 h the 9-Ch NCD-UMEA was rinsed thoroughly with distilled water to remove residues of Tergazyme and then soaked in ethyl alcohol at 70% for 2 h to obtain the sterile conditions required for cell survival. Cleaning did not damage the 9-Ch NCD-UMEA, and could be thus repeated as needed, avoiding damage or performance degradation of the device.

Results

Calibration of the 9-Ch NCD-UMEA in voltammetric and amperometric operation mode

In a preliminary series of experiments we first assayed the redox sensitivity of the microelectrode array by cyclic voltammetry using voltage ramps from 0 to +1.2 V with 20 mV/s scan rate. As shown in Fig. 2A for one representative electrode, in the presence of standard Tyrode saline solution, no redox activity was detected within the hydrolysis window (currents were <2 pA from 0 to +900 mV). Then, we tested the electrochemical response of the device in the presence of increasing

concentrations of adrenaline ([A] = 10, 100, 1000 μM) (Fig. 2B-D). We compared traces from the same representative electrode and found that the catecholamine-induced oxidation current increased proportionally with [A] to reach maximal values around +700 ÷ +900 mV. Mean maximal currents increased from 61±5 pA with 10 μM to 800±20 pA with 1 mM [A]. The NCD-UMEA was also found comparably sensitive to dopamine (100 μM) and serotonin (30 μM) (Fig. 2E, F), broadening the physiological applications of the device. We obtained mean currents of 72 ± 8 pA when 100 μM dopamine was applied and 33 ± 5 pA with 30 μM serotonin.

To quantify the sensitivity of 9-Ch NCD-UMEA to adrenaline, we set the oxidation potential to +800 mV and tested the microelectrodes responsiveness in the amperometric mode. Fig. 3A shows recordings of one representative electrode in response to 1 to 100 μM adrenaline ([A]). For each [A], data were acquired for 1 min and then the chip was washed with Tyrode solution and tested for the next concentration. The typical response of one electrode to adrenaline is shown in Fig. 3A, where only the first second of each recording are displayed sequentially, without time gaps. The sensitivity of the nine microelectrodes is shown in Fig. 3B, where is evident that all the 9 channels exhibited comparable currents, within an uncertainty of 2σ. Finally, averaged data points from Fig. 3B were fitted by linear regression (r= 0.98, slope 0.51±0.02 pA/μM), indicating direct proportionality of the amperometric response to [A] for all nine microelectrodes (Fig. 3C). For all these experiments the current values were scaled to the perimeter of the electrodes and thus to the length, since the width was the same for all electrodes. It is worth recalling that in the case of disk-shaped microelectrodes the steady-state current (I_{ss}) is proportional to the radius of the electrode (Wightman, 1981) while, in general, I_{ss} is proportional to the geometrical parameter that defines the boundary of the recording area (Sanderson & Anderson, 1985; Shea & Bard, 1987; Cohen & Kunz, 2000; Strutwolf & Williams, 2005). The general formula for calculating I_{ss} is: $I_{ss} = nFDC\Phi$, where n is the number of electrons transferred, F is the Faraday constant, D is the diffusion coefficient, C is the concentration of the redox species and Φ is the linear geometrical term defining the electrode. In our case, the geometrical parameter is the electrode length. Thus, the amperometric signals detected by the different microelectrodes were normalized to the major side of the rectangles shaping the electrodes.

Secretory events elicited in mouse chromaffin cells: the NCD-UMEA versus CFE

Exocytotic events from cultured MCCs were induced using either an electrical pulse generated by the stimulation circuitry included in the read-out electronics of the 9-Ch NCD-UMEA prototype or using KCl-enriched solutions, as previously reported using a similar boron-doped NCD-MEA (Carabelli *et al.*, 2010) or carbon fiber electrodes (CFE) (Marcantoni *et al.*, 2009; Gosso *et al.*, 2011).

In both cases, MCCs were cultured on non-adherent dishes, as previously described (Carabelli *et al.*, 2010) and then mechanically positioned on the array by means of a patch-clamp glass pipette. In this

experimental configuration, the tight contact between cell and NCD electrodes strongly limits catecholamine dilution by diffusion. The electrical stimulation was applied through all nine electrodes and consisted of a ±2 V square pulse of 50 ms. Under these conditions the release of oxidisable molecules could occur by either a depolarization of the cell in contact with the stimulation electrode or by electroporation of the plasma membrane. To identify the type of mechanism we used Trypan Blue (0.4% Sigma) staining, which allows revealing the presence of plasma membrane electroporation during stimulation (Ghosh *et al.*, 2013). We used a final 0.02% Trypan blue solution to stain the MCCs and applied trains of ±2 V square pulses of 50 ms. In n= 7 trails the cells remained unstained with no visible uptake of the dye inside the cell, suggesting no evident plasma membrane electroporation during electrical stimulation. Thus, in our case catecholamine release appears generated by a capacitative current that depolarizes the cell (Dittami & Rabbitt, 2010) and induces Ca^{2+}-driven exocytosis in form of trains of amperometric spikes of comparable size to those evoked by chemical KCl stimulation (Carabelli *et al.*, 2007; Marcantoni *et al.*, 2009; Carabelli *et al.*, 2010). Representative amperometric spikes using electrical stimulation are shown in Fig. 4A and the corresponding spike parameters are compared with recordings using KCl stimulation (Fig. 4B).

Analysis of amperometric spikes was performed using Igor macros (see (Machado *et al.*, 2001; Carabelli *et al.*, 2007) and the spike-detection criteria described in the Methods. Briefly, we measured: *1)* the maximum oxidation current (I_{max}) as the height of each spike, *2)* the vesicular charge content (Q) as the time integral of the current, *3)* the cubic root of Q ($Q^{1/3}$), which is proportional to the vesicle diameter, *4)* the rise-time of the spike 25–75% (m), *5)* the width of the spike at half of its maximum height ($t_{1/2}$) and *6)* the time to the peak (t_p). As reported in Fig. 4B, all six parameters obtained with the electrical stimulation were not statistically different from those obtained using KCl-enriched external solution ($p > 0.05$, ANOVA followed by Bonferroni post-hoc comparison).

In order to validate the device sensitivity in the presence of chromaffin cells, amperometric spikes from n= 20 MCCs were then compared with those recorded by conventional CFE (n= 21). We found that all spike parameters were not significantly different, if measured by the 9-Ch NCD–UMEA or conventional CFEs ($p > 0.05$) regardless of the type of stimulation used (electrical or KCl), indicating comparable sensitivity and time resolution of the two devices.

Mapping of amperometric spikes in bovine chromaffin cells

The geometry of the 9-Ch NCD-UMEA was designed with the specific aim of detecting secretory events from different membrane microareas of a single cell. Spatial mapping of secretory sites was performed using bovine instead of mouse chromaffin cells, due to their larger diameter (18-22 μm). In this way, the area of the central hole containing the 9 detecting microelectrodes (22 μm diameter;

Fig. 1C) was perfectly matching the size of a bovine chromaffin cell (BCCs). Representative traces of amperometric spikes using KCl-stimulated BCCs are shown in Fig. 5. Mean values of spike parameters obtained from 12 cells were then compared with those recorded by CFEs from KCl-stimulated BCCs (n= 10). As shown in Fig. 5B, there was excellent agreement among the amplitude and total charge of the spikes detected by either one of the two devices ($p > 0.05$, calculated with Student's two-tailed test), as well as in the kinetic parameters ($t_{1/2}$, m and t_p). We found that the mean $Q^{1/3}$ value, estimated with the 9-Ch-NCD-UMEA, was also in good agreement with that measured by other groups using CFEs, ranging from 1.04 ± 0.41 to 1.09 ± 0.46 $pC^{1/3}$ (Wightman *et al.*, 1991; Finnegan *et al.*, 1996; Graham *et al.*, 2000).

As an additional confirmation, we found strong similarities among the distributions of $Q^{1/3}$ and $t_{1/2}$ obtained with CFEs and 9-Ch NCD-UMEA. The double Gaussian functions required to fit the $Q^{1/3}$ distribution, were centered at 0.73 and 1.00 $pC^{1/3}$ (R^2= 0.99) for the NCD-UMEA, and at 0.64 and 0.89 $pC^{1/3}$ (R^2= 0.98) for the CFE (grey traces in Fig. 6B). Black traces represent the sum of the two single Gaussian curves. Notice that the mean charge associated with chromaffin granules fusion is approximately three-fold greater than that estimated with MCCs (0.71±0.09 pC versus 0.21±0.02 pC), in good agreement with previous reports (Graham *et al.*, 2000; Gosso *et al.*, 2011). This confirms that the 9Ch NCD–UMEA has nearly equal sensitivity to CFE.

It is worth noticing that also the kinetic parameters of the spike are in good agreement with those recorded by CFEs. Histograms of square root values of $t_{1/2}$ are shown in Fig. 6C respectively for spikes collected by the 9-Ch NCD–UMEA and CFEs. Data were collected from 12 and 10 cells, respectively, and ranged between 1.2 and 10.3 $ms^{1/2}$, for CFE and between 1.4 and 13.7 $ms^{1/2}$ with mean values of 3.7 and 3.9 $ms^{1/2}$, suggesting comparable distributions with previously reported data in BCCs using CFEs (Schroeder *et al.*, 1992; Jankowski *et al.*, 1993). Finally, we considered the parameters of amperometric spikes detected by the 9 electrodes and compared their mean values by one way ANOVA followed by a Bonferroni post-hoc analysis. We found no statistically significant differences in the spike parameters recorded with different electrodes ($p>0.05$), confirming that each of the 9 channels NCD-UMEA detects exocytotic events with the same sensitivity and resolution.

Spike frequencies revealed with the 9 Ch-NCD-MEA and CFE are comparable

We next compared the frequency of exocytotic events from MCCs when using CFEs and the 9-Ch NCD-UMEA. We obtained 0.44 ± 0.07 Hz with CFEs (n= 21 cells) and either 0.82 ± 0.18 Hz (n= 10 cells) or 0.77 ± 0.16 Hz (n= 10) with the 9-Ch NCD-UMEA when secretion was evoked by electrical-stimulation or KCl-enriched solution, respectively. Because the detection areas of the two devices was considerably different, the frequency of the events was scaled to the active surface, respectively 38.5 μm^2 (CFE) and 153 μm^2 (9-Ch NCD-UMEA). Considering that MCCs, have mean

diameter of ~15 μm and cover only 46% of the electrodes active areas, the effective biosensing area of the NCD array was proportionally reduced to 70 μm^2. Following this, the scaled frequency to the active surface of the CFEs (11.4±1.8 10^{-3} Hz/μm^2) was not significantly different from that of the 9-Ch NCD-UMEA when either using electrical (11.7 ± 2.5 Hz/μm^2) or chemical stimulation (10.9 ± 1.8 Hz/μm^2; p> 0.05, ANOVA followed by Bonferroni post-hoc comparison). Similarly, for recordings from BCCs, the spike frequency was calculated over 240 s recordings from 10 cells. Since BCCs covered the entire detection surface of the device, the scaled frequency for the two devices was 11.2±1.3 10^{-3} Hz/μm^2 for CFE and 11.1±3.9 10^{-3} Hz/μm^2 for NDC-UMEA (p> 0.05 with two-tailed Student's test), respectively.

Spatial mapping of exocytosis in bovine chromaffin cells

Given that the 9-Ch NCD-UMEA was able to reveal single vesicle release with high-time resolution, we next studied the subcellular localization of exocytotic events in bovine chromaffin cells using the Matlab routine described in the Materials and Methods. In Fig. 7 are shown the spatial localization of quantal events over the nine electrodes in 4 different BCCs. To the left are shown, on different colors, the nine electrodes drawn in an array of 44x44 square grid. The color indicates the number of quantal exocytic events detected by the sensitive area of the electrode, giving a direct chromatic view of the microdomain regions of different exocytotic activity. To the right are shown the corresponding raster plots of 2 min recordings of each electrode, as well as the occurrence of simultaneous spikes. It is evident that the 9 electrodes detected remarkably different amounts of quantal events. There were channels with intense secretory activity and channels with no activity regardless of the size of the electrode. Obviously the larger electrodes (3, 6, 9) on average detected more events. In the example of Fig. 7A (corresponding to the recordings of Fig. 5), channels 4, 5, 7 and 8 are associated to membrane domains with very low- or no-activity at all, while the remaining channels have higher activity, suggesting membrane areas with clear heterogeneous granule contents release.

As described in Materials and Methods, events were considered synchronous, and thus associated to the same secretory events, when their temporal separation was less than 10 ms. Examples of spikes simultaneous recorded from three different electrodes (1, 2 ,3) are indicated by the rectangle in the raster plot of Fig. 7A and their corresponding traces in Fig. 5. Since different electrodes detected variable amount of secretory events, independently of their active area, we quantified this variability using the *coefficient of variation* (*CV*) related to the number of events detected by the 9 channels: $CV = \frac{\sigma}{\mu} \cdot 100$, where μ is the mean of the number of events recorded individually by the nine electrodes (normalized to the surface area) and σ is the standard deviation of the mean. We found that *CV* was greater than 71% for all the cells analyzed (n= 10). In the examples of Fig. 7 the four CVs

ranged between 71% and 106%, indicating high variability of secretory activity in different areas of the cell. Notice that in the case of extreme homogeneity (when each electrode reveals the same normalized number of events) the expected *CV* is zero.

We should also remark that although secretion regularly occurred in all cells tested (n= 10), 22 of the total 90 channels analyzed remained silent (white bar in Fig 8A), corresponding to 24% of channels unable to detect secretory activity (Fig. 8B). From the histogram of the percentage of release recorded from each channel (Fig. 8A) it is evident that there are surface areas of very different activity. The histogram exhibits two clear minima around 30 and 65% that suggest the existence of areas that we intuitively defined of *no-* or *low-activity* with percentage of secretion below 30% (white and light-blue bars in Fig. 8A), *medium-activity* with secretion between 30 and 65% (green bars) and *high-activity* with secretion above 65%. Excluding the channels with no-activity (*silent*; 24%), we found that on average all the other microelectrodes recorded an almost equal percentage of *low-* (22%), *medium-* (26%) and *high-activity* (28%) (Fig. 8B). We also noticed that, although covering only 28% of the total area, the channels exhibiting *high-activity* (dark-red colors) covered a continuous narrow area that crossed the cell along the diameter (see right panels in Fig. 7). This cell-crossing area of *high-activity* seems a peculiarity of BCCs. It was observed in 8 of the 10 cells tested and occurred at different angular orientation (see the examples in Fig. 7), as expected due to the casual positioning of the cell on the chip.

In conclusions, secretion in BCCs viewed through the 9-Ch NCD-UMEA appears remarkably heterogeneous and organized in large microdomains. Activity is absent in 24% of the cell surface ("*silent zones*") and coexists with well-defined continuous areas of intense activity covering nearly the same percentage of cell surface (28%). Areas of *high-* and *medium-activity* cover more or less half of the cell surface (54%) comparable to the remaining 46% exhibiting either *low-* or *no-activity*. Thus, the new picture of chromaffin cells that we derive from the 9-Ch NCD-UMEA is of a cell with large fractions of non-secreting areas under physiological conditions whose structural organization and functional role remain to be investigated.

Discussion

Here we propose an improved version of a 9-Ch NCD-UMEA to resolve neurotransmitter secretion within microdomains of single chromaffin cells. Specifically, the new microchip is: *i)* suitable for multisite recordings within single living cells, *ii)* responsive to micromolar neurotransmitter concentrations, and *iii)* versatile in both chronoamperometric and voltammetric mode. The multisite array highlights the existence of large microdomains with *high*, *medium* and *low* secretory activity as well as areas of *silent zones* with null activity in BCCs. On average, each region of activity and silent

zones cover nearly 1/4 of the total area. The high-activity area seems to extend transversally along the cell diameter, suggesting the existence of a highly polarized secretory area, evocative of the arrangement of the intact gland, where chromaffin cells are packed in column facing the capillary (Carmichael, 1987; Garcia *et al.*, 2006). This "*secretory pole*" may be preserved in isolated cells and gives origin to the "*high-activity zones*" that are randomly oriented due to the casual cell positioning on the chip.

Another interesting finding with the 9-Ch NCD-UMEA is that only half of the cell surface exhibits high-medium secretory activity (54%), while the remaining 46% is either silent or weakly responding to stimulation. The "*silent zones*" are randomly distributed and occupy 24% of the total surface area. Areas lacking secretion have been already reported in BCCs using small tip diameter CFEs (2 μm) (Schroeder *et al.*, 1994; Robinson *et al.*, 1995), but a quantitative estimation of the covered areas was biased by the complexity of monitoring secretion by randomly moving two small-size CFEs under the microscope. This issue can be now more easily tackled by the 9-Ch NCD-MEA, given its planar configuration and high-resolution sensitive areas. It is worth noticing, however, that the present distribution of "hot" and "silent" zones in isolated cells may be different in adrenal-gland slices or *in-vivo* conditions.

Planar boron-doped diamonds vs. other chips for electrochemical signaling

Despite their high-time resolution and low-background noise (Chow *et al.*, 1992), CFEs can be hardly used for simultaneous fluorescence imaging and patch-clamping and their use is limited to the anodic range. Thus, other materials and geometries have been proposed to fabricate electrochemical biosensors with improved performances. Lindau's lab was the first to adopt a planar array of Pt-microelectrodes to investigate vesicles localisation and fusion pore formation (Dias *et al.*, 2002; Hafez *et al.*, 2005; Berberian *et al.*, 2009) and, more recently, arrays of indium-tin-oxide (ITO), nitrogen-doped diamond-like carbon and thin gold films on glass substrates, with improved transparency (Kisler *et al.*, 2012). All arrays were capable of detecting amperometric signals with high resolution except ITO, which showed significantly lower sensitivity to catecholamines. An improved spatial resolution was recently achieved using microelectrode tips containing 8-15 carbon-ring fibers to detect amperometric signals from individual neurons or cell networks (Zhang *et al.*, 2008; Lin *et al.*, 2012). In good agreement with our findings, Lin *et al.* (2012) found that secretion in PC12 is extremely heterogeneous when recorded with an 8 carbon-ring microelectrode array (CRMA) of 20 μm total diameter. They found evidence for microareas of high-activity as well as "*cold-spots*" of low- or no-activity, which remained silent for more than 3 min. In PC12 cells 1 out of 8 channels was silent, while we found on average 2.2 channels out of 9 not responding in BCCs.

Despite these differences, it is interesting to underscore how the increased spatial resolution with arrays of 8-9 sensitive microareas per cell helps to uncover microdomains of "no secretion" (*silent zones*) which are overlooked in devices with one or few microelectrodes per cell surface. "*Inactive release zones"* were first reported by Schroeder *et al.* (1994), using small-diameter CFEs moved on top of BCCs surface.

The 9-Ch NCD-UMEA for resolving amperometric spikes in cell microdomains

As previously reported, the main advantages of using boron-doped NCD-UMEAs to record amperometric signals are: the electrochemical stability, the large hydrolysis window, robustness, the transparency from the far infrared to UV and the possibility of using CVD, photolitography and dry etching techniques to construct microarrays of defined geometries (Gao *et al.*, 2010; Colombo *et al.*, 2011). With respect to our previous NCD prototypes (Carabelli *et al.*, 2010; Pasquarelli *et al.*, 2011) here we provide an advanced array geometry to spatially identify microdomains of neurosecretion in single chromaffin cells. Amperometric signals collected from MCCs and BCCs with the 9-Ch NCD-MEAs exhibited no significant difference from those recorded by CFEs, which represent the "gold standard" for this approach. Mean amperometric charges are in good agreement with those measured by others using CFEs (Finnegan *et al.*, 1996; Haller *et al.*, 1998), thus confirming that the 9-Ch chip is sensitive enough for detecting the release of quantal fusion events from chromaffin cells.

Considering the high-density geometry of the array and that chromaffin cells were positioned and held on the detector surface by a patch-pipette, a tight contact of the cell to the electrode was ensured. This reduces the rate-limiting diffusional dispersion of catecholamines (Jankowski *et al.*, 1993) and optimizes their amperometric detection. In this regard, the estimated spike half-width is comparable with that measured by CFEs (14 ms with 9-Ch NCD-UMEA vs. 8-18 ms with CFEs) (Haller *et al.*, 1998) and with the mean value estimated by Pt-microelectrodes (13.8 ms) (Berberian *et al.*, 2009). Distribution of the $t_{1/2}$ square root values (Schroeder *et al.*, 1992) measured by the 9-Ch NCD-UMEA confirms that also spike duration is comparable with that of CFEs, thus confirming the excellent time-resolution of the diamond chip.

Our findings also suggest that quantal events recorded from the apex (with CFEs) or from the bottom of a chromaffin cell (with the 9-Ch NCD-UMEA) are comparable. This is in good agreement with recordings from cell bottom using planar arrays of different materials and geometry, and confirms the convenience of using planar microchips for detecting secretion (Chen *et al.*, 1994; Hafez *et al.*, 2005; Gao *et al.*, 2010; Picollo *et al.*, 2013). However, these observations are at variance with previous findings on BCCs (Amatore *et al.*, 2007), reporting different secretion efficiency between the apex

and the bottom of the cell using ITO devices. An explanation for this discrepancy could be due to the different cell plating conditions, besides the materials and the electrode geometry.

Spatial mapping of exocytosis with the 9-Ch NCD-UMEA

Our data clearly show that secretory granules can be independently detected by all the electrodes of the 9-Ch NCD-UMEA. Some electrode detected high-medium secretory activity, while others low- or no-activity. The two areas covered more or less half of the cell, but most interestingly, 2.2 channels out of 9 remained silent, uncovering a remarkably heterogeneous spatial mapping of exocytosis in BCCs. The physiological meaning of the highly localized areas for secretion and large areas of silent activity remains to be clarified. A possibility is that secretion is highly polarized in the columnar organization of chromaffin cells in the intact gland. Chromaffin cells are innervated at one site and face blood capillaries at another site, which is presumably the "*secretory pole*", since most of the vesicles are found there (Carmichael, 1987). If this geometry is preserved in isolated cells, it will give origin to the random diametrically distributed crossing-area of high-activity illustrated in Fig. 7. There could be obviously other explanations to the existence of high-activity areas, but it is clear that the 9-Ch NCD-MEA opens new perspectives through which secretion can be studied at higher spatial resolution and pose new questions on how the different cell micro-domains are organized in terms of Ca^{2+} channels densities, SNARE proteins availability, vesicle pools distribution. An intriguing possibility is that the "*silent areas*" may undergo remodeling of ion channels, membrane receptors and membrane proteins controlling secretion (Guerineau *et al.*, 2012) and become active during chronic stress or sustained neurogenic stimulation of the adrenal gland. New versions of the chip with an increased number of ultra-microelectrodes and improved transparency would certainly enhance the interest on this new nanotech approach allowing simultaneous measurements of secretion and fluorescence imaging and other parameters that diamond chips can measure in potentiometric mode (action potentials, pH) (Bitziou *et al.*, 2008).

A final concern on the potential use of 9-Ch NCD-MEA is related to the present dimensions of the electrodes which are 3 to 10 times larger than the 2 µm diameter CFEs (Schroeder *et al.*, 1994). These dimensions do not allow to draw any conclusion on how secretion is organized, neither in CNS synapses, where docked vesicles are tightly coupled to presynaptic Ca^{2+} channels in nanodomains (Schneggenburger *et al.*, 2012), nor in chromaffin cells where Ca^{2+} channels and secretory granules are either co-localized in μm^2 hot-spots (Monck *et al.*, 1994; Robinson *et al.*, 1995; Wu *et al.*, 2009) or uniformly distributed over membrane areas where Ca^{2+} channels are loosely coupled to chromaffin granules (Klingauf & Neher, 1997; Carabelli *et al.*, 1998). Our findings suggest that, independently of the coupling of chromaffin granules to Ca^{2+} channels, exists a macroscopic heterogeneity

associated with the existence of large domains of cell surface where secretion is either absent or low for about half of the total area.

References

Amatore C, Arbault S, Lemaitre F & Verchier Y. (2007). Comparison of apex and bottom secretion efficiency at chromaffin cells as measured by amperometry. *Biophysical chemistry* **127,** 165-171.

Ayers S, Berberian K, Gillis KD, Lindau M & Minch BA. (2010). Post-CMOS fabrication of working electrodes for on-chip recordings of transmitter release. *IEEE transactions on biomedical circuits and systems* **4,** 86-92.

Barizuddin S, Liu X, Mathai JC, Hossain M, Gillis KD & Gangopadhyay S. (2010). Automated targeting of cells to electrochemical electrodes using a surface chemistry approach for the measurement of quantal exocytosis. *ACS chemical neuroscience* **1,** 590-597.

Berberian K, Kisler K, Fang Q & Lindau M. (2009). Improved surface-patterned platinum microelectrodes for the study of exocytotic events. *Analytical chemistry* **81,** 8734-8740.

Bitziou E, O'Hare D & Patel BA. (2008). Simultaneous detection of pH changes and histamine release from oxyntic glands in isolated stomach. *Analytical chemistry* **80,** 8733-8740.

Carabelli V, Carra I & Carbone E. (1998). Localized secretion of ATP and opioids revealed through single Ca2+ channel modulation in bovine chromaffin cells. *Neuron* **20,** 1255-1268.

Carabelli V, Gosso S, Marcantoni A, Xu Y, Colombo E, Gao Z, Vittone E, Kohn E, Pasquarelli A & Carbone E. (2010). Nanocrystalline diamond microelectrode arrays fabricated on sapphire technology for high-time resolution of quantal catecholamine secretion from chromaffin cells. *Biosensors & bioelectronics* **26,** 92-98.

Carabelli V, Marcantoni A, Comunanza V, de Luca A, Diaz J, Borges R & Carbone E. (2007). Chronic hypoxia up-regulates alpha1H T-type channels and low-threshold catecholamine secretion in rat chromaffin cells. *The Journal of physiology* **584,** 149-165.

Carmichael SW. (1987). *Morphology and innervation of the adrenal medulla.*, vol. 1. CRC Press, Boca Raton, Florida.

Chen TK, Luo G & Ewing AG. (1994). Amperometric monitoring of stimulated catecholamine release from rat pheochromocytoma (PC12) cells at the zeptomole level. *Analytical chemistry* **66,** 3031-3035.

Chow RH, von Ruden L & Neher E. (1992). Delay in vesicle fusion revealed by electrochemical monitoring of single secretory events in adrenal chromaffin cells. *Nature* **356,** 60-63.

Cohen AE & Kunz RR. (2000). Large-area interdigitated array microelectrodes for electrochemical sensing. *Sensors and Actuators B-Chemical* **62,** 23-29.

Colombo E, Men Y, Scharpf J, Pietzka C, Dipalo M, Herfurth P, Gao Z, Schneider M, Carabelli V, Carbone E, Kohn E & Pasquarelli A. (2011). Fabrication of a NCD microelectrode array for amperometric detection with micrometer spatial resolution. *Diamond and Related Materials* **20,** 793-797.

Dias AF, Dernick G, Valero V, Yong MG, James CD, Craighead HG & Lindau M. (2002). An electrochemical detector array to study cell biology on the nanoscale. *Nanotechnology* **13,** 285-289.

Dittami GM & Rabbitt RD. (2010). Electrically evoking and electrochemically resolving quantal release on a microchip. *Lab on a chip* **10,** 30-35.

Finnegan JM, Borges R & Wightman RM. (1996). Comparison of cytosolic Ca2+ and exocytosis responses from single rat and bovine chromaffin cells. *Neuroscience* **71,** 833-843.

Gao Z, Carabelli V, Carbone E, Colombo E, Demaria F, Dipalo M, Gosso S, Manfredotti C, Pasquarelli A, Rossi S, Xu Y, Vittone E & Kohn E. (2010). Transparent diamond microelectrodes for biochemical application. *Diamond and Related Materials* **19,** 1021-1026.

Gao Z, Carabelli V, Carbone E, Colombo E, Dipalo M, Manfredotti C, Pasquarelli A, Feneberg M, Thonke K, Vittone E & Kohn E. (2011). Transparent microelectrode array in diamond technology. *Journal of Micro-Nano Mechatronics* **6,** 33-37.

Garcia AG, Garcia-De-Diego AM, Gandia L, Borges R & Garcia-Sancho J. (2006). Calcium signaling and exocytosis in adrenal chromaffin cells. *Physiol Rev* **86,** 1093-1131.

Gerhardt G & Adams RN. (1982). Determination of diffusion coefficients by flow injection analysis. *Analytical chemistry* **54,** 2618-2620.

Ghosh J, Liu X & Gillis KD. (2013). Electroporation followed by electrochemical measurement of quantal transmitter release from single cells using a patterned microelectrode. *Lab on a chip* **13,** 2083-2090.

Gosso S, Gavello D, Giachello CN, Franchino C, Carbone E & Carabelli V. (2011). The effect of CdSe-ZnS quantum dots on calcium currents and catecholamine secretion in mouse chromaffin cells. *Biomaterials* **32,** 9040-9050.

Graham ME, Fisher RJ & Burgoyne RD. (2000). Measurement of exocytosis by amperometry in adrenal chromaffin cells: effects of clostridial neurotoxins and activation of protein kinase C on fusion pore kinetics. *Biochimie* **82,** 469-479.

Guerineau NC, Desarmenien MG, Carabelli V & Carbone E. (2012). Functional Chromaffin Cell Plasticity in Response to Stress: Focus on Nicotinic, Gap Junction, and Voltage-Gated Ca2+ Channels. *Journal of Molecular Neuroscience* **48,** 368-386.

Hafez I, Kisler K, Berberian K, Dernick G, Valero V, Yong MG, Craighead HG & Lindau M. (2005). Electrochemical imaging of fusion pore openings by electrochemical detector arrays. *Proc Natl Acad Sci U S A* **102,** 13879-13884.

Haller M, Heinemann C, Chow RH, Heidelberger R & Neher E. (1998). Comparison of secretory responses as measured by membrane capacitance and by amperometry. *Biophysical journal* **74,** 2100-2113.

Jankowski JA, Schroeder TJ, Ciolkowski EL & Wightman RM. (1993). Temporal characteristics of quantal secretion of catecholamines from adrenal medullary cells. *The Journal of biological chemistry* **268,** 14694-14700.

Kim BN, Herbst AD, Kim SJ, Minch BA & Lindau M. (2012). Parallel recording of neurotransmitters release from chromaffin cells using a 10x10 CMOS IC potentiostat array with on-chip working electrodes. *Biosensors & bioelectronics* **41,** 736-744.

Kisler K, Kim BN, Liu X, Berberian K, Fang Q, Mathai CJ, Gangopadhyay S, Gillis KD & Lindau M. (2012). Transparent electrode materials for simultaneous amperometric detection of exocytosis and fluorescence microscopy. *Journal of biomaterials and nanobiotechnology* **3,** 243-253.

Klingauf J & Neher E. (1997). Modeling buffered Ca2+ diffusion near the membrane: Implications for secretion in neuroendocrine cells. *Biophysical journal* **72,** 674-690.

Lin Y, Trouillon R, Svensson MI, Keighron JD, Cans AS & Ewing AG. (2012). Carbon-ring microelectrode arrays for electrochemical imaging of single cell exocytosis: fabrication and characterization. *Analytical chemistry* **84,** 2949-2954.

Machado JD, Morales A, Gomez JF & Borges R. (2001). cAmp modulates exocytotic kinetics and increases quantal size in chromaffin cells. *Molecular pharmacology* **60,** 514-520.

Marcantoni A, Carabelli V, Vandael DH, Comunanza V & Carbone E. (2009). PDE type-4 inhibition increases L-type Ca(2+) currents, action potential firing, and quantal size of exocytosis in mouse chromaffin cells. *Pflugers Archiv : European journal of physiology* **457,** 1093-1110.

Monck JR, Robinson IM, Escobar AL, Vergara JL & Fernandez JM. (1994). Pulsed laser imaging of rapid Ca2+ gradients in excitable cells. *Biophysical journal* **67,** 505-514.

Pasquarelli A, Carabelli V, Xu Y, Colombo E, Gao Z, Scharpf J, Carbone E & Kohn E. (2011). Diamond microelectrodes arrays for the detection of secretory cell activity. *International Journal of Environmental Analytical Chemistry* **91,** 150-160.

Picollo F, Gosso S, Vittone E, Pasquarelli A, Carbone E, Olivero P & Carabelli V. (2013). A new diamond biosensor with integrated graphitic microchannels for detecting quantal exocytic events from chromaffin cells. *Advanced materials (Deerfield Beach, Fla)* **25,** 4696-4700.

Robinson IM, Finnegan JM, Monck JR, Wightman RM & Fernandez JM. (1995). Colocalization of calcium entry and exocytotic release sites in adrenal chromaffin cells. *Proc Natl Acad Sci U S A* **92,** 2474-2478.

Sanderson DG & Anderson LB. (1985). Filar electrodes - steady-state currents and spectroelectrochemistry at twin interdigitated electrodes. *Analytical chemistry* **57,** 2388-2393.

Schneggenburger R, Han Y & Kochubey O. (2012). Ca(2+) channels and transmitter release at the active zone. *Cell calcium* **52,** 199-207.

Schroeder TJ, Jankowski JA, Kawagoe KT, Wightman RM, Lefrou C & Amatore C. (1992). Analysis of diffusional broadening of vesicular packets of catecholamines released from biological cells during exocytosis. *Analytical chemistry* **64,** 3077-3083.

Schroeder TJ, Jankowski JA, Senyshyn J, Holz RW & Wightman RM. (1994). Zones of exocytotic release on bovine adrenal medullary cells in culture. *The Journal of biological chemistry* **269,** 17215-17220.

Shea TV & Bard AJ. (1987). Digital-simulation of homogeneous chemical-reactions coupled to heterogeneous electron-transfer and applications at platinum mica platinum ultramicroband electrodes. *Analytical chemistry* **59,** 2101-2111.

Staal RG, Mosharov EV & Sulzer D. (2004). Dopamine neurons release transmitter via a flickering fusion pore. *Nat Neurosci* **7,** 341-346.

Strutwolf J & Williams DE. (2005). Electrochemical sensor design using coplanar and elevated interdigitated array electrodes. A computational study. *Electroanalysis* **17,** 169-177.

Wightman RM. (1981). Microvoltammetric electrodes. *Analytical chemistry* **53,** 1125A-1134A.

Wightman RM, Jankowski JA, Kennedy RT, Kawagoe KT, Schroeder TJ, Leszczyszyn DJ, Near JA, Diliberto EJ, Jr. & Viveros OH. (1991). Temporally resolved catecholamine spikes correspond to single vesicle release from individual chromaffin cells. *Proc Natl Acad Sci U S A* **88,** 10754-10758.

Wightman RM, Schroeder TJ, Finnegan JM, Ciolkowski EL & Pihel K. (1995). Time course of release of catecholamines from individual vesicles during exocytosis at adrenal medullary cells. *Biophysical journal* **68,** 383-390.

Wu MM, Llobet A & Lagnado L. (2009). Loose coupling between calcium channels and sites of exocytosis in chromaffin cells. *The Journal of physiology* **587,** 5377-5391.

Xin Q & Wightman RM. (1998). Simultaneous detection of catecholamine exocytosis and Ca2+ release from single bovine chromaffin cells using a dual microsensor. *Analytical chemistry* **70,** 1677-1681.

Zhang B, Adams KL, Luber SJ, Eves DJ, Heien ML & Ewing AG. (2008). Spatially and temporally resolved single-cell exocytosis utilizing individually addressable carbon microelectrode arrays. *Analytical chemistry* **80,** 1394-1400.

Competing interests
None.

Author contributions

S.G., C.F. and V.C. contributed to data collection and analysis of amperometric and voltammetric experiments, performed in the laboratories of the Department of Drug Science at the University of Torino, Italy. A.P. and El.Co. contributed to the design and production of the 9-Ch NCD-UMEA and to the hardware and software development, at the Department of Electron Devices and Circuits, University of Ulm. S.G. and M.T. developed the MatLab routine for the localization of the amperometric events. S.G., Em.Ca. and V.C. contributed to the conception and design of experiments and the drafting of the article as well as revising it critically for important intellectual content. All authors have approved the final version of the manuscript.

Fundings

This work was supported by Regione Piemonte, P.O.R.-F.E.S.R. 2008/2014 project “Be-Free” and P.O.R.-F.E.S.R. 2007/2013 project “MicroDiBi”; by the Italian Ministry for University and Research (MIUR), “FIRB-Futuro in Ricerca 2010” project D11J11000450001, and PRIN 2010/2011 project 2010JFYFY2.

Figure Legends

Figure 1. The 9-Ch NCD MEA geometry

A) Chip assembly into the carrier board. B) Detail of connecting carrier and the perfusion chamber C) Geometry of the electrode array: the whole surface is passivated with the exception of the circular central area, in which are radially patterned the nine electrodes contacting the gold strips (dark tracks). On the left a patch-clamp pipette has been used to place a mouse chromaffin cell on the electrodes.

Figure 2. Voltametric configuration: responses to catecholamines

Cyclic voltammetric recordings from 0 to +1.2 V are shown for one representative electrode in the presence of a Tyrode standard solution *(A)*, and Tyrode solution plus: *B)* adrenaline 10 μM, *C)* adrenaline 100 μM, *D)* adrenaline 1 mM, *E)* dopamine 100 μM, *F)* serotonin 30 μM. Insets in *A)* and *B)* show an enlarged view of CV limited to the range which is relevant for oxidation.

Figure 3. Amperometric configuration: sensitivity to adrenaline

A) Amperometric responses to adrenaline at the indicated concentrations are shown for a representative electrode, polarized to + 800 mV. Traces of one electrode over 120 seconds total recording have been selected. For each concentration is shown only the first second of the recording. Consecutive recordings using increasing concentrations of adrenaline were separated by time breaks (not indicated in the figure), in order to properly remove the previous solution and wash the device. *B)* Mean values and SD of amperometric response obtained from the nine channels at the concentrations indicated. Inset provides an enlarged view at low adrenaline concentrations. *C)* Linear regression line through the averaged data taken from B (R = 0.98; see text).

Figure 4. Detection of quantal events from mouse chromaffin cells

A) Representative amperometric spikes from a MCC detected by the nine microelectrodes, indicated as Ch 1 to Ch 9. A single spike detected by electrode 8 (Ch 8) enlarged on the time scale, is shown in the inset. *B)* Mean values of spike parameters and related standard errors averaged from n= 21 MCCs for CFEs and n= 10 MCCs for 9-ch NCD UMEA for either KCl and electrical stimulation. Data referring to the maximal current amplitude (Imax), quantal charge (Q) and its cubic root ($Q^{1/3}$), rising phase slope (m), half time width ($t_{1/2}$), time to peak (t_p) are compared for CFEs and 9-Ch NCD-UMEA.

Figure 5. Detection of quantal events from bovine chromaffin cells

A) Representative amperometric spikes from a BCC detected by the nine microelectrodes, indicated as Ch 1 to Ch 9. A single spike detected by electrode 6 (Ch 6), enlarged on the time scale, is shown

in the inset. Notice the low- or no release activity of Ch 4, 5 and 8 *B)* Mean values of spike parameters averaged averaged from n=10 bovine chromaffin cells for CFEs and n=12 bovine chromaffin cells for 9 ch NCD MEA. Data referring to maximum current amplitude (I_{max}), quantal charge (Q) and its cubic root ($Q^{1/3}$), rising phase slope (m), half time width ($t_{1/2}$), time to peak (t_p) and normalized frequency to the detection area (f_{norm}) are compared for CFEs and 9-Ch NCD-UMEA.

Figure 6. Spike size and kinetics comparison: CFEs recordings vs. 9-Ch NCD-UMEA

A) Representative amperometric spikes detected by one channel of the 9-Ch NCD-UMEA (left) and by a CFE (right) using bovine chromaffin cells. Notice the "foot" anticipating the fast rising phase of the two amperometric spikes. *B)* Cubic root charge histogram distribution fitted by a double Gaussian function derived from the 9-Ch NCD-UMEA (left) and CFE (right) spike recordings (see text for details of the fitting). C) Half-time width histogram derived from the 9-Ch NCD-UMEA (left) and CFE (right) spike recordings.

Figure 7. Spatial mapping of exocytosis in BCCs viewed by the 9-Ch NCD-UMEA

A-D) Examples of the heterogeneous exocytosis recorded in four individual BCCs placed on top of the 9-Ch NCD-UMEA. The panels to the left illustrate the geometry of the 9 recording channels. The colors indicate the number of secretory events recorded by each electrode in 2 min. Data of panel *A* are derived from the recordings of Fig. 5A. The middle panels are the corresponding raster plots of the amperometric recordings which generate the color to the left. For each example, the coefficient of variation (*CV*) of the recorded events is indicated. To the right are shown the manual reconstructions of the *high-activity* areas (*brown*) derived from the panels to the left as they would appear in a round BCC. The *light-blue* areas indicate the rest of the surface area which displays (*medium*, *low* and *no activity).*

Figure 8. Histogram of the percentage of release revealed by the 9-Ch NCD-UMEA and percentage of surface areas with different secretory activities

A) Histogram of the percentage of release detected by each of the nine ultra-microelectrodes collected from ten BBCs for a total of 90 recording channels. The colors indicate different percentage of activity: *no-activity* (white bar), *low-activity* (light-blue); *medium-activity* (green) and *high-activity* (dark-red). *B*) Percentage of the channel areas recording either *no-release* (white), *low-* (light-blue), *medium-* (green) and *high-secretory activity* (dark-red) (see text for details).

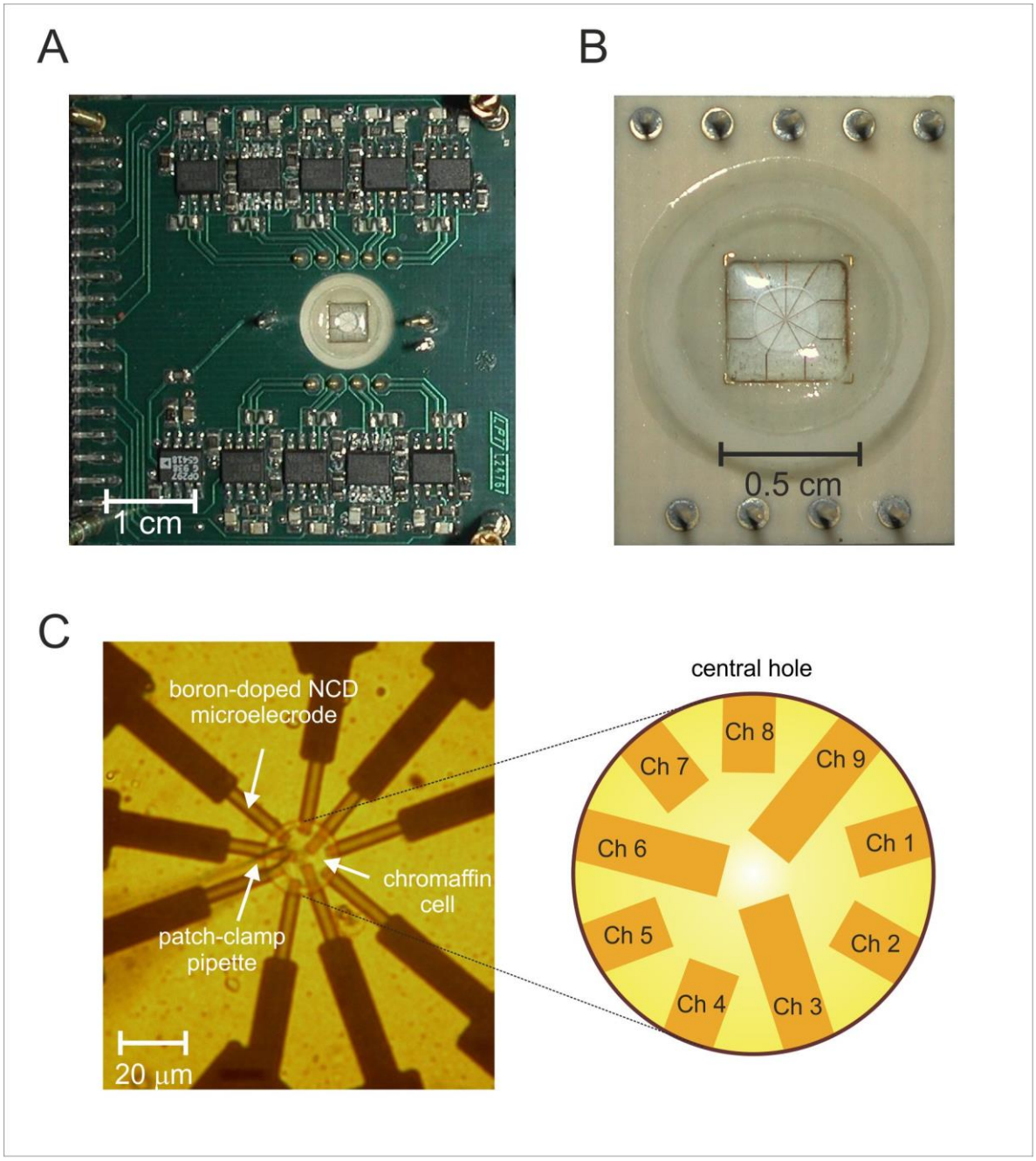

Gosso et al., Figure 1

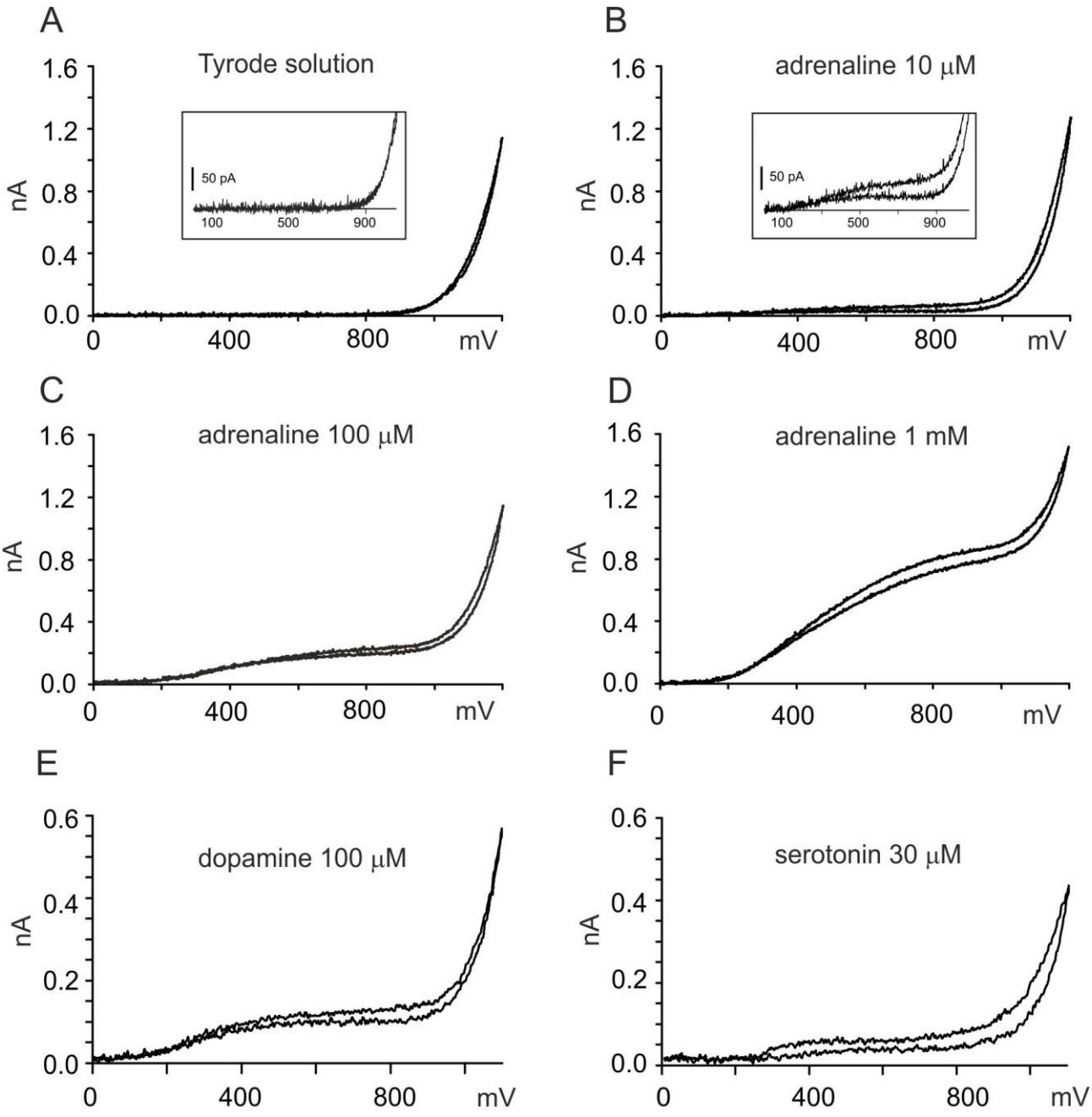

Gosso et al., Figure 2

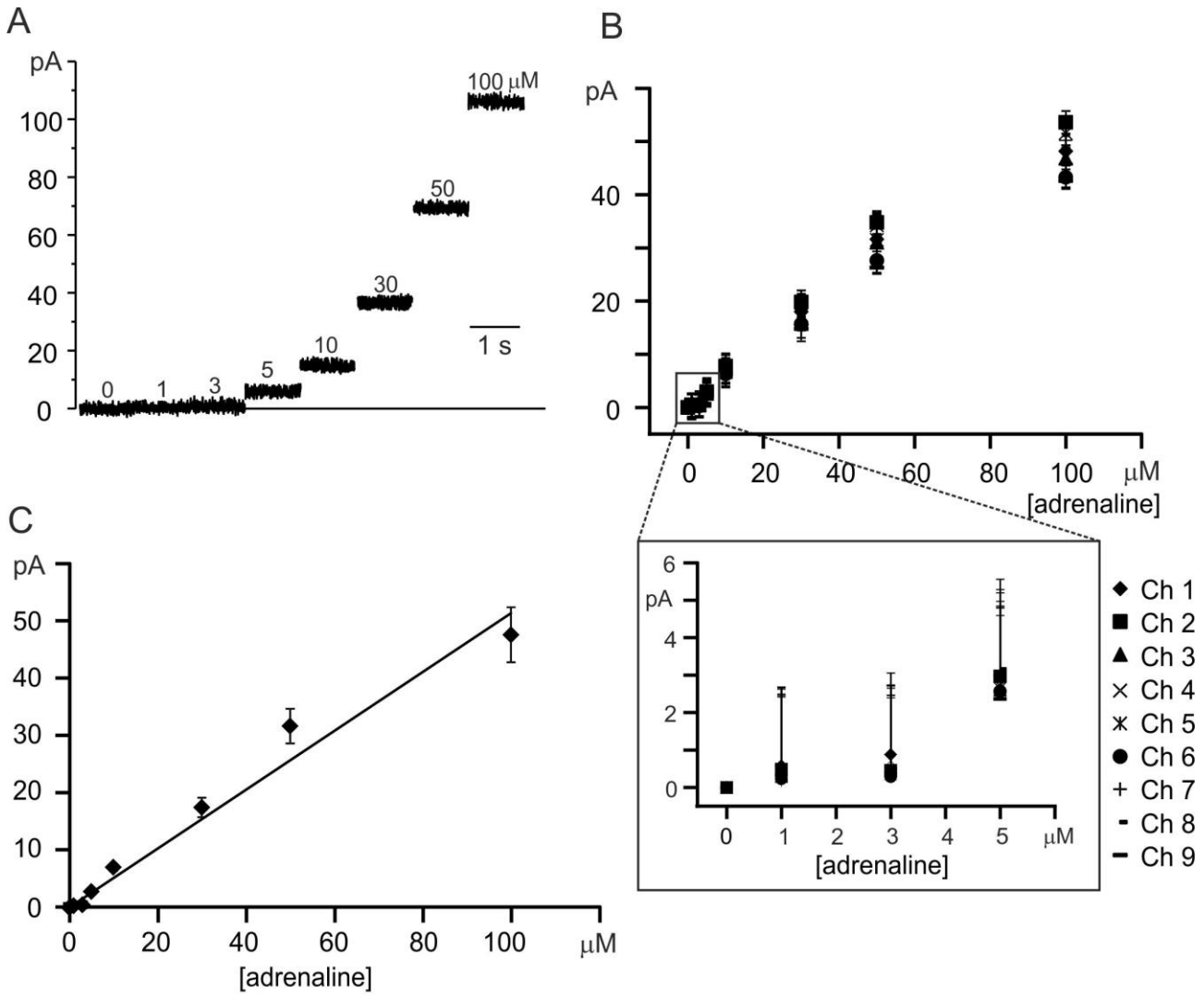

Gosso et al., Figure 3

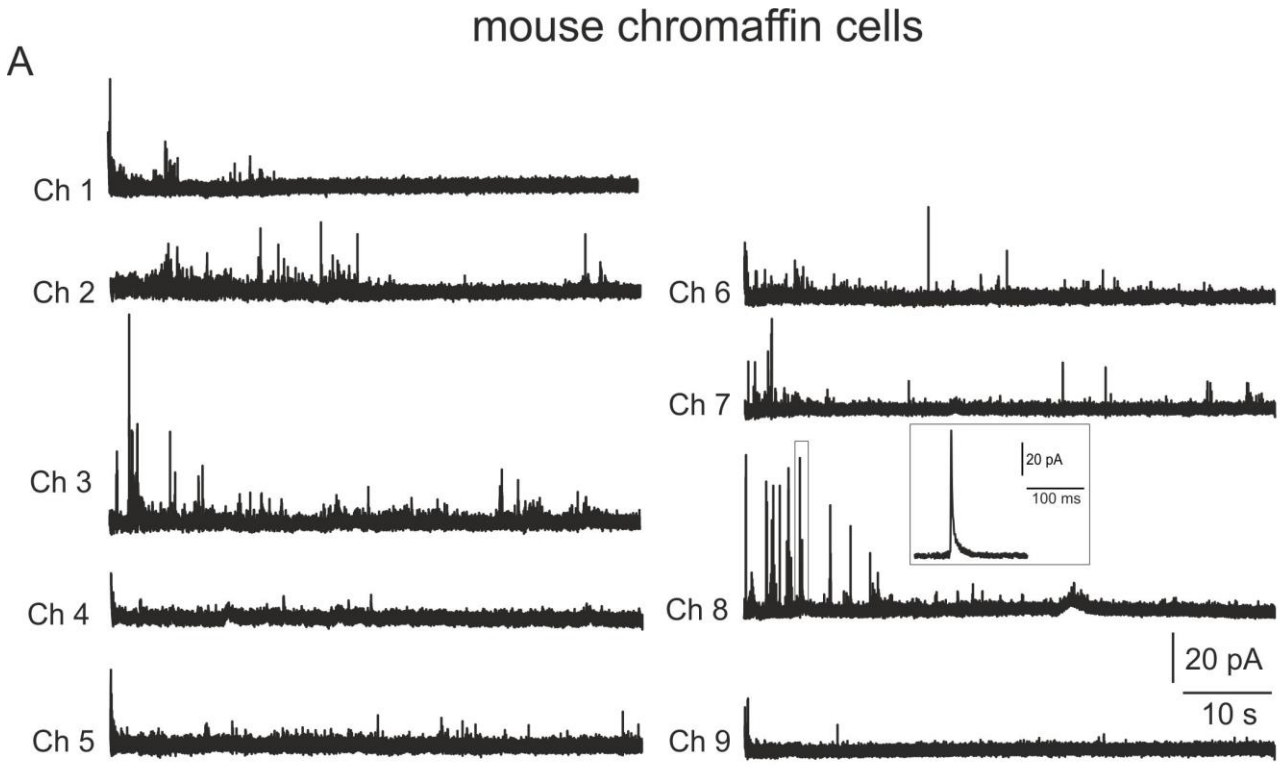

B

parameter	CFE(KCl)	NCD-UMEA(KCl)	NCD-UMEA (elect.)
Imax (pA)	33±3	26±2	27±3
Q (pC)	0.21±0.02	0.30±0.03	0.24±0.08
$Q^{1/3}$ ($pC^{1/3}$)	0.52±0.01	0.62±0.04	0.53±0.05
m (nA/s)	14.5±1.5	11±1	11.9±1.8
$t_{1/2}$ (ms)	6.4±0.3	8±1	7±2
t_p (ms)	4.3±0.2	4.4±0.4	4.4±1.1

Gosso et al., Figure 4

A

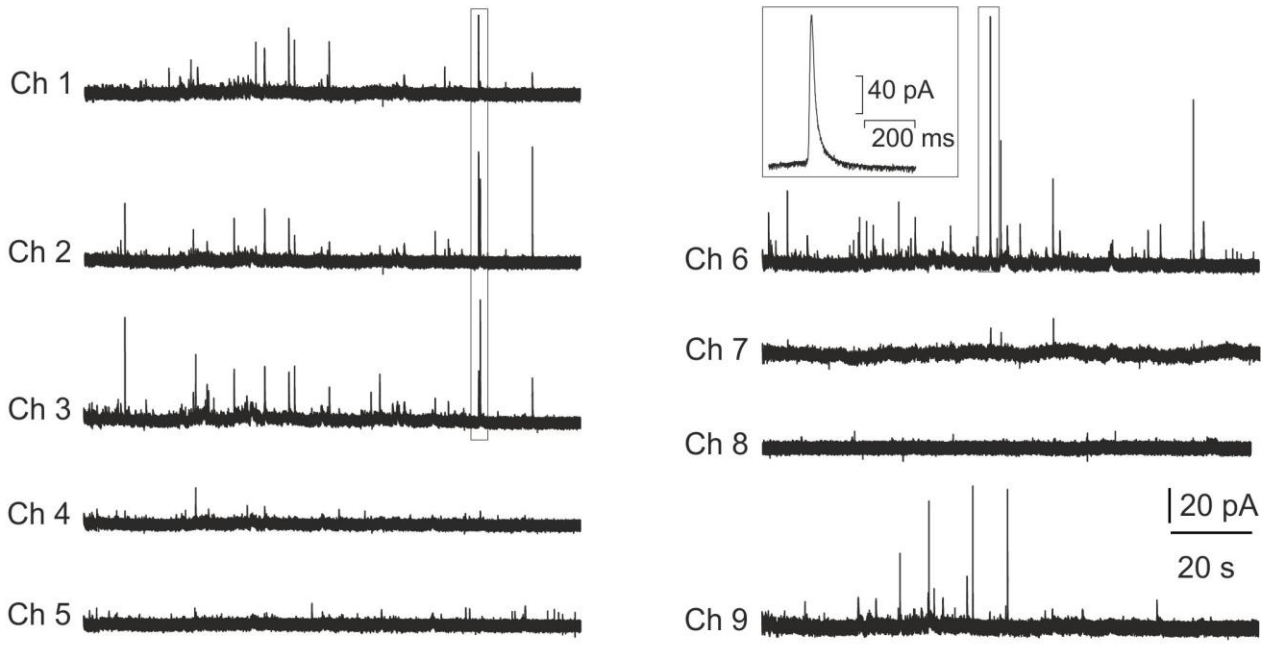

B

parameter	CFE(KCl)	NCD-UMEA(KCl)
Imax (pA)	52±3	44±3
Q (pC)	0.71±0.09	0.91±0.15
$Q^{1/3}$ ($pC^{1/3}$)	0.78±0.03	0.88±0.04
m (nA/s)	18.2±1.7	13.1±1.9
$t_{1/2}$ (ms)	14.0±1.5	15.1±1.7
t_p (ms)	6.9±0.5	6.6±0.6

Gosso et al., Figure 5

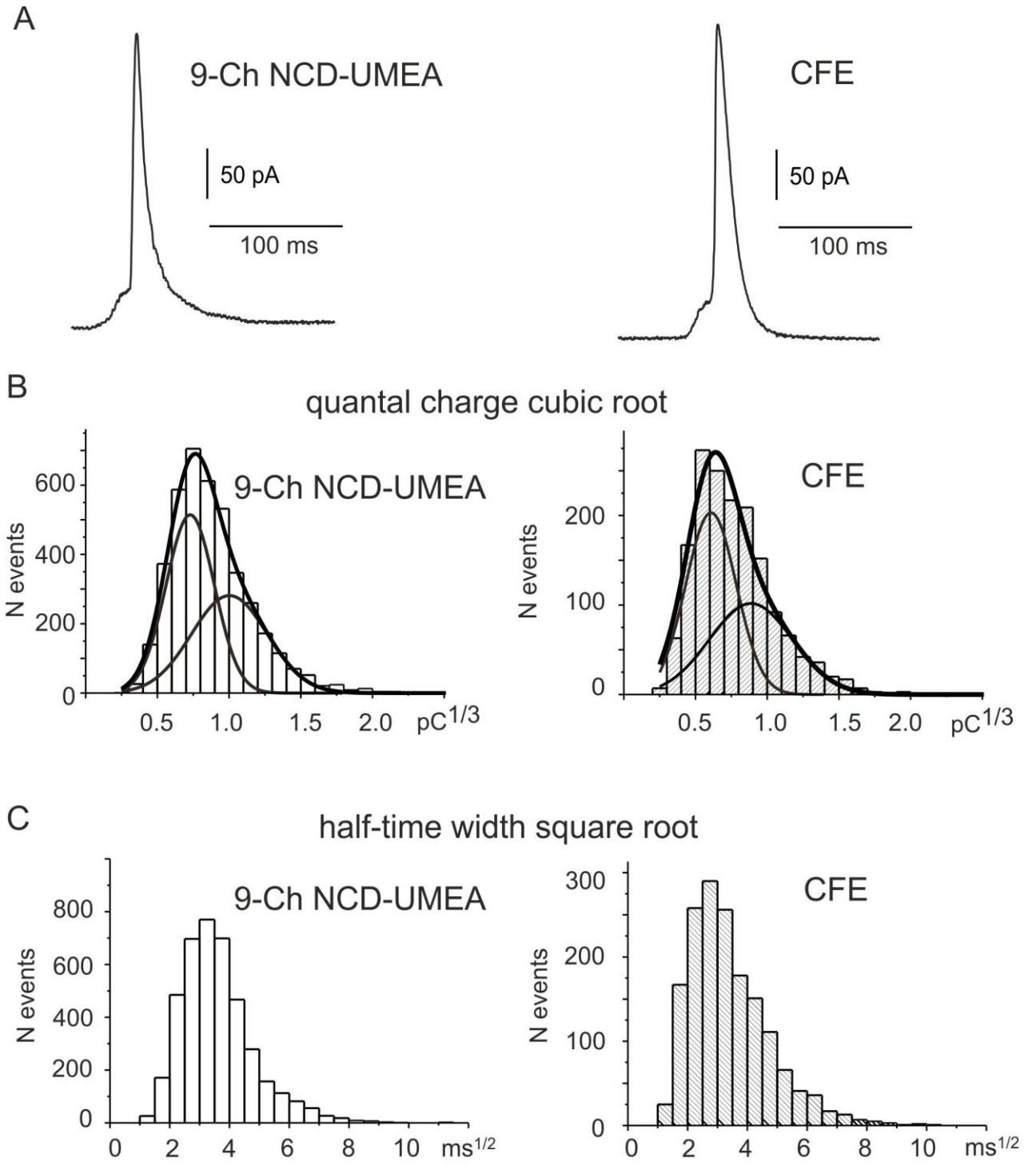

Gosso et al., Figure 6

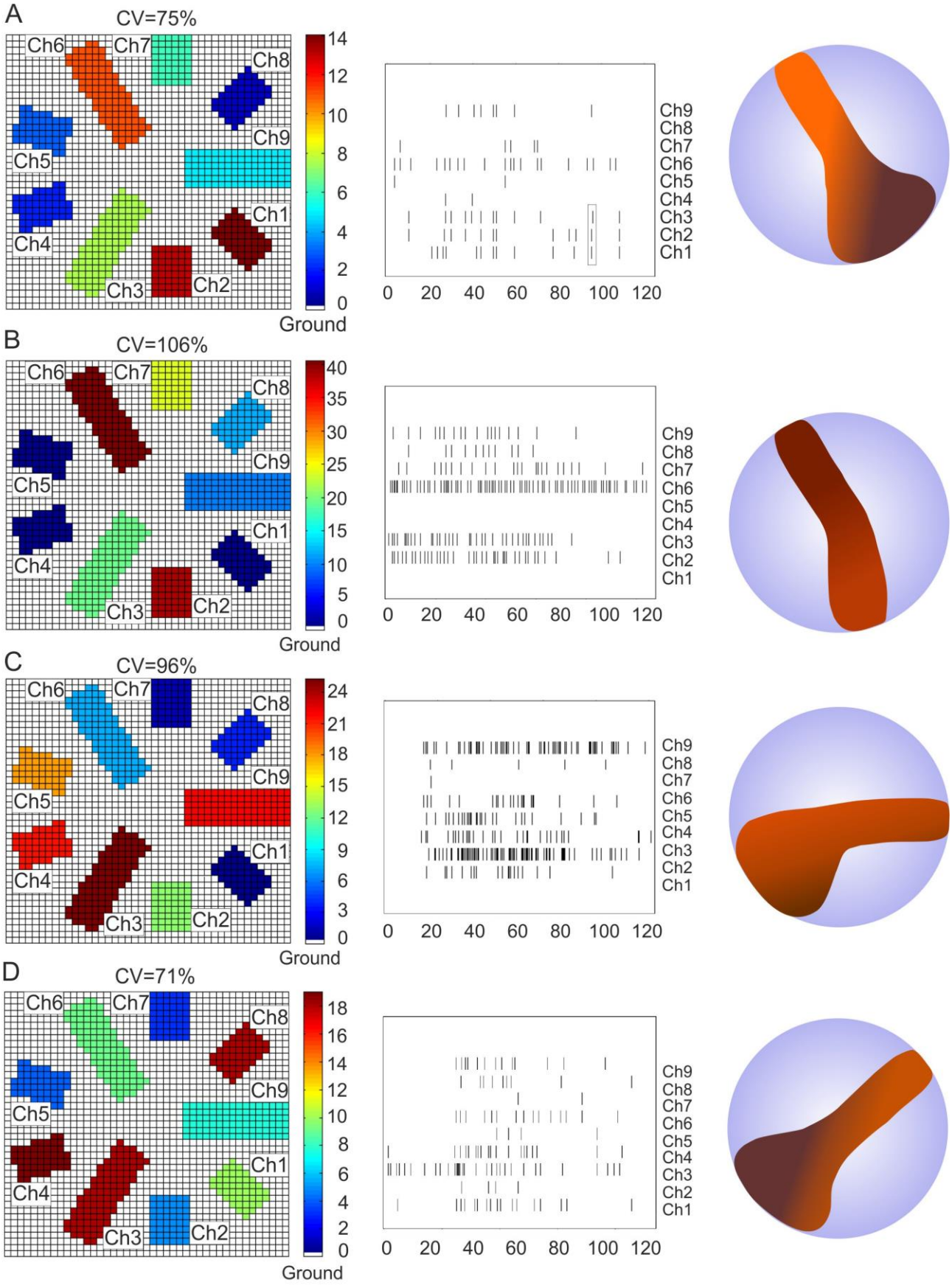

Gosso et al., Figure 7

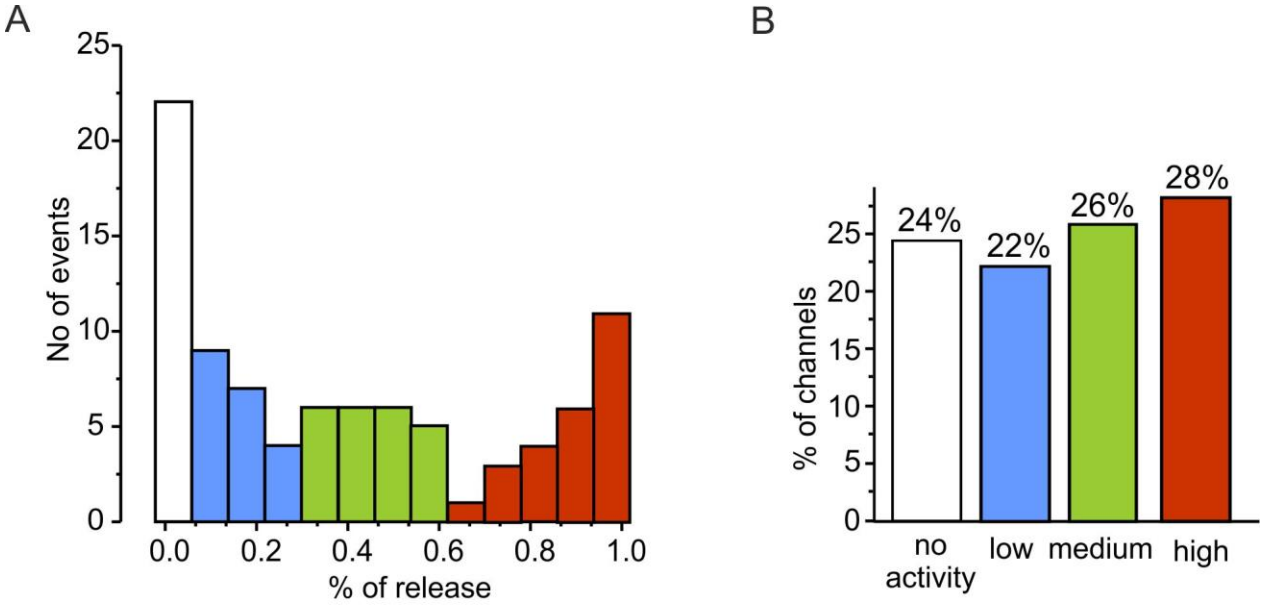

Gosso et al., Figure 8